

CM² MAGAZINE



第 121 期



南方科技大学海洋磁学中心主编

<http://cm2.sustech.edu.cn/>

创刊词

海洋是生命的摇篮，是文明的纽带。地球上最早的生命诞生于海洋，海洋里的生命最终进化成了人类，人类的文化融合又通过海洋得以实现。人因海而兴。

人类对海洋的探索从未停止。从远古时代美丽的神话传说，到麦哲伦的全球航行，再到现代对大洋的科学钻探计划，海洋逐渐从人类敬畏崇拜幻想的精神寄托演变成可以开发利用与科学研究的客观存在。其中，上个世纪与太空探索同步发展的大洋科学钻探计划将人类对海洋的认知推向了崭新的纬度：深海（deep sea）与深时（deep time）。大洋钻探计划让人类知道，奔流不息的大海之下，埋藏的却是亿万年的地球历史。它们记录了地球板块的运动，从而使板块构造学说得到证实；它们记录了地球环境的演变，从而让古海洋学方兴未艾。

在探索海洋的悠久历史中，从大航海时代的导航，到大洋钻探计划中不可或缺的磁性地层学，磁学发挥了不可替代的作用。这不是偶然，因为从微观到宏观，磁性是最基本的物理属性之一，可以说，万物皆有磁性。基于课题组的学科背景和对海洋的理解，我们对海洋的探索以磁学为主要手段，海洋磁学中心因此而生。

海洋磁学中心，简称 CM^2 ，一为其全名“Centre for Marine Magnetism”的缩写，另者恰与爱因斯坦著名的质能方程 $E = MC^2$ 对称，借以表达我们对科学巨匠的敬仰和对科学的不懈追求。

然而科学从来不是单打独斗的产物。我们以磁学为研究海洋的主攻利器，但绝不仅限于磁学。凡与磁学相关的领域均是我们关注的重点。为了跟踪反映国内外地球科学特别是与磁学有关的地球科学领域的最新研究进展，海洋磁学中心特地主办 CM^2 Magazine，以期与各位地球科学工作者相互交流、合作共进！

“海洋孕育了生命，联通了世界，促进了发展”。21 世纪是海洋科学的时代，由陆向海，让我们携手迈进中国海洋科学的黄金时代。

目录

1. 碳都去哪儿了?	2
2. 大陆溢流玄武岩喷发之前的全球变暖	4
3. 中国东部新生代造山运动及其与亚洲气候格局重组的关系	7
4. 干旱与社会变化:伊斯兰教在古代阿拉伯出现的环境背景	10
5. 与矿物学相关的全球土壤有机碳储存和容量	13
6. 阿曼钻探项目超镁铁质岩芯的一个新的岩石磁学分析及其对下地壳和上地幔蚀变的意义	15
7. 法国南部普罗旺斯二叠纪脊椎动物足迹以及对晚卡匹敦陆地灭绝事件的暗示	17
8. 中国西南地区全新世火灾史与气候变化及人类活动有关	20
9. 末次冰期太平洋水体在塔斯曼深部的外流	23
10. 晚全新世中国北方半干旱地区植被变化从自然向人为强迫的过渡	26

1. 碳都去哪儿了？

翻译人：仲义 zhongy@sustech.edu.cn



Denning, A.S., *Where has all the carbon gone? [JJ]. Annual Review of Earth and Planetary Science, 2022, 50, 55-78.*

<https://www.annualreviews.org/doi/abs/10.1146/annurev-earth-032320-092010>

摘要：碳作为宇宙中最丰富的物质之一，虽然在地球上已经严重枯竭，但它仍然是生物化学中的主要结构元素。碳和气候之间的复杂相互作用使得地球系统在地质历史内逐渐稳定下来。从 20 世纪 50 年代开始现代观测记录二氧化碳以来，约有一半的化石燃料排放并被海洋和陆地生态所封存。海洋对化石 CO₂ 的吸收受到生物地球化学和环流的控制。而陆地生态系统净吸收能力令人惊讶，因为它在全球范围持续性增强超过衰退能力。陆地生态系统主要通过 (a) CO₂ 施肥作用，(b) 氮肥，(c) 农业废弃后森林的恢复作用以及 (d) 北方变暖。陆地和海洋的碳汇都受到了气候变暖的威胁，并且由于先前储存的碳的不断释放加剧气候变化，碳汇能力可能会减弱，甚至逆转。而化石燃料产生的 CO₂ 在停止排放后将持续存在几个世纪，甚至几千年。

ABSTRACT: Carbon is among the most abundant substances in the universe; although severely depleted on Earth, it is the primary structural element in biochemistry. Complex interactions between carbon and climate have stabilized the Earth system over geologic time. Since the modern instrumental CO₂ record began in the 1950 s, about half of fossil fuel emissions have been sequestered in the oceans and land ecosystems. Ocean uptake of fossil CO₂ is governed by chemistry and circulation. Net land uptake is surprising because it implies a persistent worldwide excess of growth over decay. Land carbon sinks include (a) CO₂ fertilization, (b) nitrogen fertilization, (c) forest regrowth following agricultural abandonment, and (d) boreal warming. Carbon sinks in both land and oceans are threatened by warming and are likely to weaken or even reverse as emissions fall with the potential for amplification of climate change due to the release of previously stored carbon. Fossil CO₂ will persist for centuries and perhaps many millennia after emissions cease.

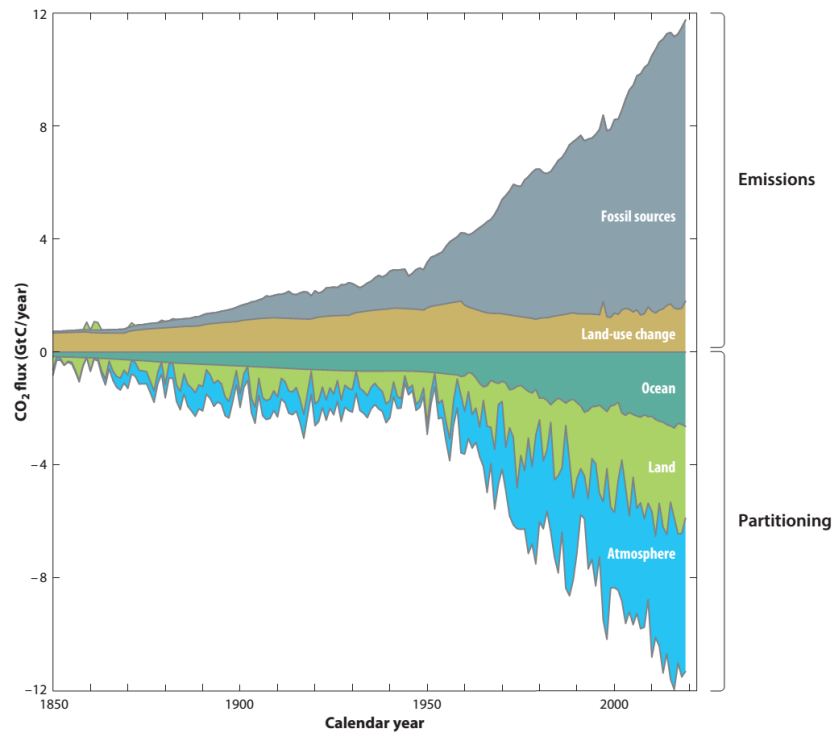


Figure 1. Combined components of the global carbon budget illustrated as a function of time, for fossile CO₂ emission (gray) and from land-use change (brown), as well as their partitioning among the atmosphere (blue), ocean (turquoise), and land (green). Abbreviation: GtC, gigatons carbon. Figure adapted from Friedlingstein et al. (2020).

2. 大陆溢流玄武岩喷发之前的全球变暖

翻译人：周洋 zhouy3@sustech.edu.cn



Tian, X.C. & Buck, W.R. *Intrusions induce global warming before continental flood basalt volcanism [JJ]. Nature Geoscience, 2022,15:417-422.*

<https://doi.org/10.1038/s41561-022-00939-w>

摘要：生物灭绝事件与大陆溢流玄武岩的喷发有关。这些玄武岩喷发产生的大量碳排放可能对全球气候和生物圈造成灾难性影响。来自德干高原和哥伦比亚河玄武岩的高精度地质年代学表明，全球变暖的开始时间比溢流玄武岩喷发的主要阶段早了数十万年。在这里，我们构建了岩床侵入的数值模型，来研究气候变暖和玄武岩喷发之间的这种滞后效应。该模型根据地壳密度和温度结构来确定岩床侵入的深度。当岩床侵入体以上的平均密度大于岩浆密度时，就会发生大规模喷发。当与碳循环模拟相结合时，这些模型可以拟合与德干高原和哥伦比亚河玄武岩群相关的全球变暖事件的时间和幅度。因此，我们得出结论，大陆溢流玄武岩的主要喷发需要大量玄武质岩浆侵入使地壳致密化。这种喷发前的侵入体结晶可以释放足够的二氧化碳，在溢流玄武岩火山活动主要喷发之前引发全球变暖。

ABSTRACT: Extinction events are known to correlate with continental flood basalt eruptions. Massive carbon degassing from these eruptions can have catastrophic impacts on the global climate and biospheres. However, high-precision geochronology from the Deccan Traps and the Columbia River Basalt Group suggests that the onset of global warming precedes the main phase of flood basalt eruptions by several hundred thousand years. Here we construct a numerical model of sill intrusion to investigate this lag between warming and eruptions. The model determines the depth of sill intrusion depending on the evolving crustal density and temperature structures. Main-phase eruptions occur when the average density above the sill intrusion is greater than the magma density. When combined with a carbon-cycle simulation, the models can reproduce the observed timing and amplitude of the global warming events associated with the Deccan Traps and the Columbia River Basalt Group. We therefore conclude that major eruptions of continental flood basalts require densification of the crust by voluminous basaltic

magma intrusions. The crystallization of such pre-eruption intrusions could release enough carbon dioxide to drive substantial global warming before the main phase of flood basalt volcanism.

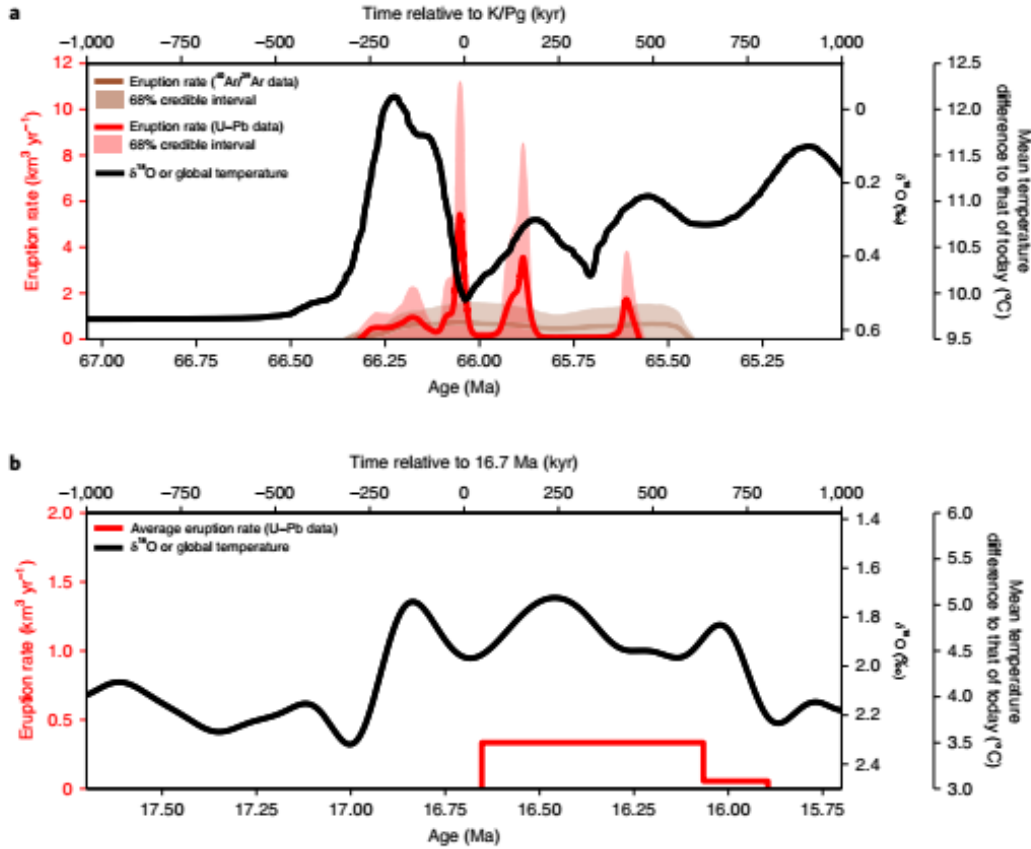


Figure 1. Global temperature variations within 1,000 kyr of the approximate onset of the main volcanic phases of the Deccan Traps and CRBG10 LIPs. a,b, The Deccan Traps (a) and CRBG–MCO (b) Cretaceous–Palaeogene (K/Pg) global warming. The black lines are $\delta^{18}\text{O}$ data or estimated temperature variations with time. For the Deccan Traps, the eruption rates with their corresponding 68% credible intervals are from ref. 50. Details of the geochronology models and temperature estimates are described in the Supplementary Information. Note the different scales for the eruption rate in a and b.

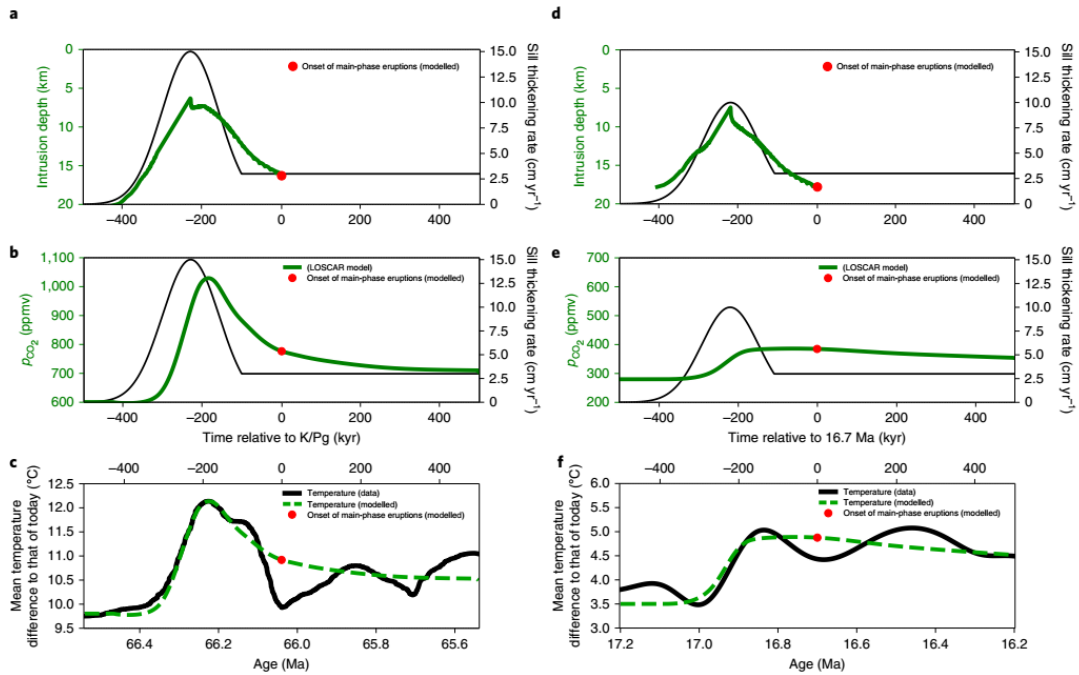


Figure 2. Time series of modelled global temperature variations and onsets of the main-phase eruptions of Deccan Traps and CRBG. a–f, Time series for the main-phase eruptions of the Deccan Traps around the K/Pg (a–c) and of CRBG and MCO (d–f). a,d, Sill intrusion depth and the timing of transition from mostly intrusion to main-phase eruptions, predicted by the thermomechanical model described in Methods, given the indicated melt flux with time. The CRBG case (d) has a lower peak sill thickening rate of 10 cm yr⁻¹. b,e, Global averaged atmospheric CO₂ concentration with time predicted by the LOSCAR climate model. c,f, global temperature change predicted by the LOSCAR model on top of climate data (Fig. 1) and with the modelled timing of the onsets of main-phase eruptions. See the Supplementary Information for details of the LOSCAR model set-up.

3. 中国东部新生代造山运动及其与亚洲气候格局重组的关系

翻译人: 刘伟 inewway@163.com



Yu, J, Zheng, D, Pang, J. et al. *Cenozoic mountain building in eastern China and its correlation with reorganization of the Asian climate regime[J]. Geology, 2022.*

<https://doi.org/10.1130/G49917.1>

摘要: 新生代亚洲气候系统在古近纪-新近纪之交经历了由区域型气候模式向季风气候型模式的转变。青藏高原的隆升、副特提斯洋的回退、南海的扩张和大气中 CO₂ 含量的降低等一系列机制被认为是亚洲气候模式转变的主要原因。然而,中国东部地区地形变化的作用却很少被考虑。作为地理、气候和生物的自然分界线,中国东部最明显的两组地形---秦岭和太行山---在塑造亚洲气候格局中发挥着重要作用。本文报告了秦岭和太行山的低温热年代学数据结果,基于年龄-海拔关系和热历史模型的研究,表明这两个山脉在渐新世晚期和中新世早期都经历了一个快速剥露的阶段。秦岭和太行山在渐新世-中新世之交的造山运动在时间和空间上与亚洲新生代气候格局的重组相对应,表明中国东部造山运动可能是亚洲新生代气候格局重组的驱动机制。

ABSTRACT: The Cenozoic Asian climate system experienced a transformation from a zonal pattern to a monsoon-dominant pattern around the Paleogene-Neogene boundary. A series of dynamic mechanisms, such as uplift of the Tibetan Plateau, retreat of the Paratethys Sea, expansion of the South China Sea, and decreasing atmospheric CO₂ content, has been suggested to be responsible for the transformation of the Asian climate pattern. However, the role of topographic growth in eastern China has been rarely considered. As the natural divides of geography, climate, and biology, the two most distinct sets of topographic relief in eastern China, the Qinling and Taihang Mountains, play an important role in shaping the Asian climate pattern. We report low-temperature thermochronology data from the Qinling and Taihang Mountains and use age-elevation relationships and thermal history modeling to show that both mountain ranges experienced a phase of rapid exhumation during the late Oligocene and early Miocene. The building of the Qinling and

Taihang Mountains around the Oligocene-Miocene boundary temporally and spatially coincided with the reorganization of the Cenozoic Asian climate regime, suggesting that the mountain building in eastern China acted as a possible driving mechanism for the alleged reorganization of the Cenozoic Asian climate regime.

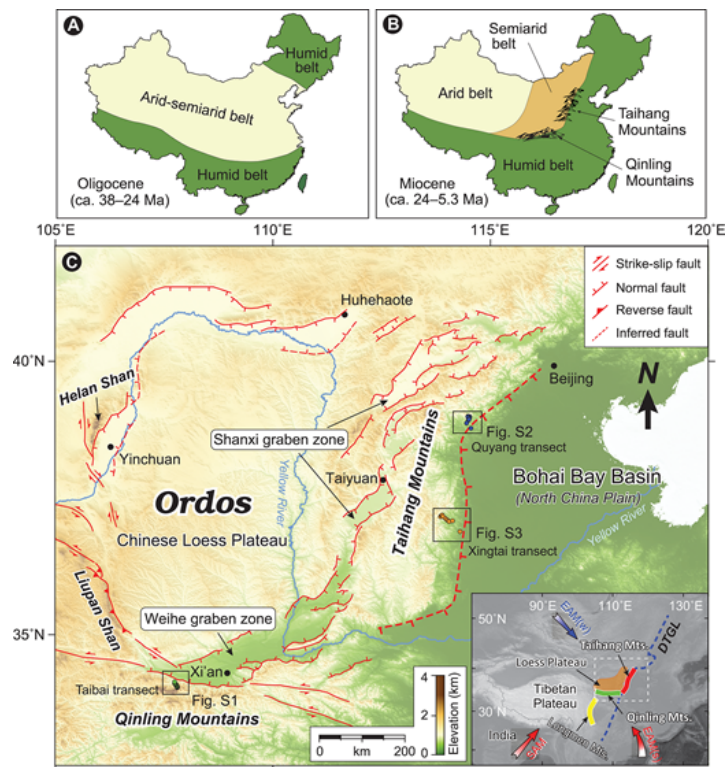


Figure 1. (A, B) Paleoenvironment pattern in China during the Oligocene (A) and Miocene (B) based on depositional, palynological, and paleobotanical data. Modified from Guo et al. (2008). (C) Relief map of the Ordos block and North China Plain with major late Quaternary active faults and the locations of three thermochronological sampling transects (Taibai [green], Quyang [blue], and Xingtai [orange]) (See Figs. S1–S3 in the Supplemental Material [see footnote 1]). White dashed rectangle in the inset shows the location of panel C. Locations of the Taihang (red), Qinling (green), and Longmen (yellow) Mountains are shown in the inset. EAM(w)—East Asian winter monsoon; EAM(s)—East Asian summer monsoon; SAM—South Asian monsoon; DTGL—Daxing’anling-Taihang gravity lineament.

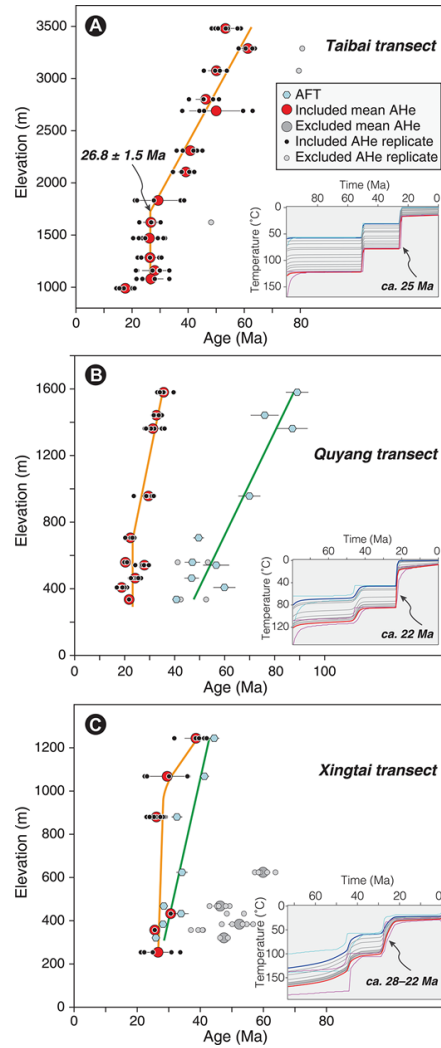


Figure 2. Age-elevation relationship for the thermochronological data from the Taibai (A), Quyang (B), and Xingtai (C) transects (see Fig. 1C for transect locations). Error bars show 1σ analytical uncertainties for single-grain apatite (U-Th)/He (AHe) ages and 1σ standard deviation for mean AHe ages. Orange and green lines are the inferred tendency of AHe and apatite fission-track (AFT) ages, respectively. QTQt modeling (<http://iearth.edu.au/codes/QTQt/>) thermal histories are shown in the inset for each transect. Thermal histories of the uppermost and lowermost samples are plotted in thick blue and red, respectively. Thin blue and red lines show 95% confidence intervals. More-detailed explanations on thermal modeling results are provided in the Supplemental Material (see footnote 1); AHe and AFT dating results are given in Tables S1–S3.

4. 干旱与社会变化:伊斯兰教在古代阿拉伯出现的环 境背景

翻译人: 杨会会 11849590@mail.sustech.edu.cn



Fleitmann, D., Haldon, J., Bradley, R.S. et al., Droughts and societal change: The environmental context for the emergence of Islam in late Antique Arabia [J]. Science, 2022, 376, 1317-1321

<https://doi.org/10.1126/science.abg4044>

摘要: 公元 6 世纪上半叶, 统治着阿拉伯社会直到公元 525 年的希米亚灭亡。随后发生了重要的社会和政治变化, 促进了主要的阿拉伯政治的解体。在这里, 我们提供了阿拉伯南部附近的水文气候记录, 包括来自阿曼北部的一份新的高分辨率石笋记录。这些记录清楚地表明, 公元 6 世纪发生了前所未有的干旱, 最严重的干旱持续在公元 500 年至 530 年之间。我们认为, 这样的干旱破坏了希亚尔的恢复, 从而促成了伊斯兰教产生的社会变革。

ABSTRACT: In Arabia, the first half of the sixth century CE was marked by the demise of Himyar, the dominant power in Arabia until 525 CE. Important social and political changes followed, which promoted the disintegration of the major Arabian polities. Here, we present hydroclimate records from around Southern Arabia, including a new high-resolution stalagmite record from northern Oman. These records clearly indicate unprecedented droughts during the sixth century CE, with the most severe aridity persisting between ~500 and 530 CE. We suggest that such droughts undermined the resilience of Himyar and thereby contributed to the societal changes from which Islam emerged.

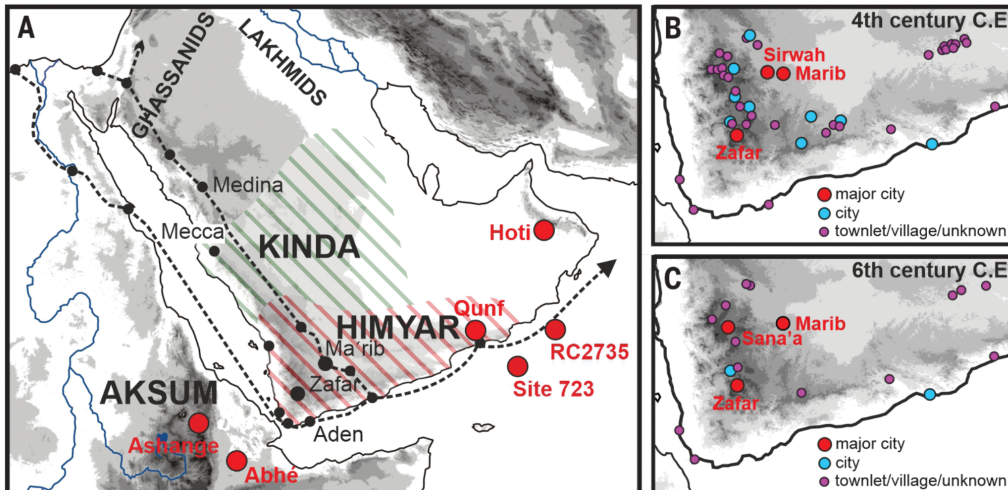


Figure 1. Location and settlement maps. (A) Map showing the location of key proxy records and the suggested extent of Himyar (red line) and Kinda (green line) at the beginning of the sixth century CE. Black dashed lines denote the main trading routes. (B and C) Settlement patterns in Himyar in the (B) fourth and (C) sixth centuries CE.

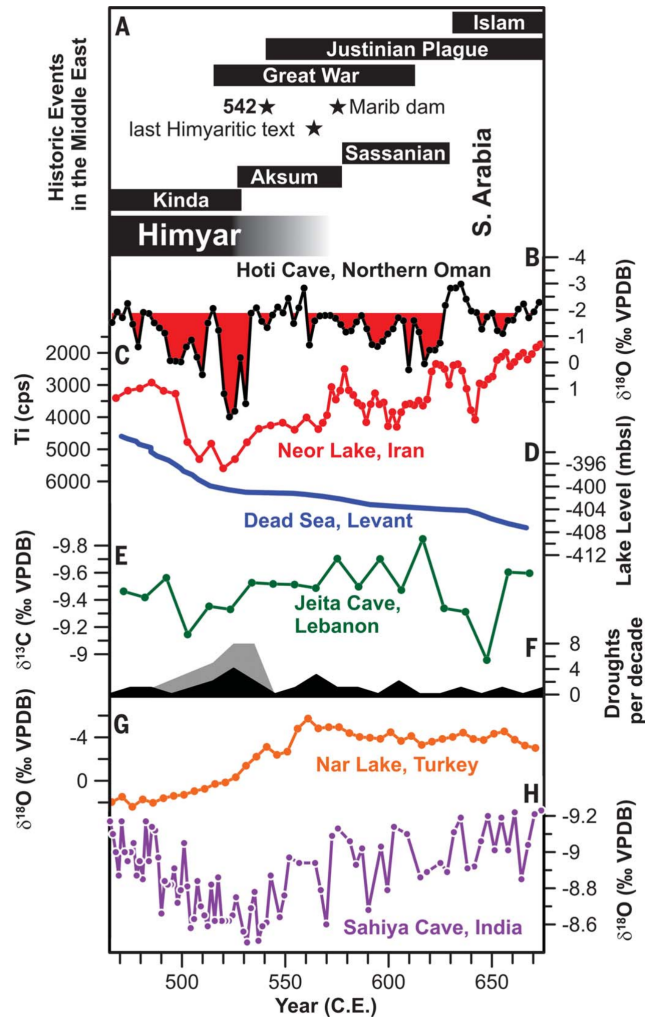


Figure 2. Climate proxy records and historic events. (A) Key historic and cultural events in southern Arabia. Black bars denote ruling powers in southern Arabia, sociocultural events (star symbols) such as the disappearance of Himyarite inscriptions, and the destruction of the dam of Marib. (B) H12 $\delta^{18}\text{O}$ record from Hoti Cave. The red-shaded area marks periods of below-normal precipitation (with respect to the 1978-1997 average of -1.8‰). (C) Lake Neor titanium record from Iran. cps, counts per second. (D) Dead Sea level. mbsl, meters below sea level. (E) Jeita Cave $\delta^{13}\text{C}$ record. (F) Historic accounts (plotted as droughts per decade) derived from the Middle East after (black-shaded curve) and (gray-shaded curve). (G) Nar Lake $\delta^{18}\text{O}$ record from Turkey. (H) Sahiya Cave $\delta^{18}\text{O}$ record from India.

5. 与矿物学相关的全球土壤有机碳储存和容量

翻译人: 王敦繁 Dunfan-w@foxmail.com



Georgiou, K., Jackson, R.B., Vindušková, O. et al. *Global stocks and capacity of mineral-associated soil organic carbon [JJ]. Nat Commun 13, 3797 (2022).*

<https://doi.org/10.1038/s41467-022-31540-9>

摘要: 土壤是最大的陆地有机碳储存库,对减缓气候变化和碳气候反馈至关重要。土壤碳与矿物的化学和物理联系在碳储存中发挥着关键作用,但这种形式的碳储存量和全球容量仍未定量。在这里,我们通过分析 1144 个全球分布的土壤剖面,得出了与矿物相关的有机碳储量和碳存储容量的空间分辨率全球估计。我们表明,目前在非永久冻土的矿物土壤中总储量为 899 Pg C,深度约为 1 m。虽然它分别占表层和深层土壤碳的 66%和 70%,但只占矿物学容量的 42%和 21%。农业活动区和较深土层中与矿物相关的碳欠饱和程度最大。重要的是,欠饱和的程度表明了多年到几十年的整合效率。我们的研究表明,在全球管理干预措施的 103 项碳积累测量中,与矿物相关的土壤碳积累最有效;在容量为十分之一的土壤中,其固存率平均比容量为二分之一的土壤高出三倍。我们的研究结果为理解世界土壤分布、土壤储存碳的能力、土壤碳管理的优先区域提供了见解。

ABSTRACT: Soil is the largest terrestrial reservoir of organic carbon and is central for climate change mitigation and carbon-climate feedbacks. Chemical and physical associations of soil carbon with minerals play a critical role in carbon storage, but the amount and global capacity for storage in this form remain unquantified. Here, we produce spatially-resolved global estimates of mineral-associated organic carbon stocks and carbon-storage capacity by analyzing 1144 globally-distributed soil profiles. We show that current stocks total 899 Pg C to a depth of 1 m in non-permafrost mineral soils. Although this constitutes 66% and 70% of soil carbon in surface and deeper layers, respectively, it is only 42% and 21% of the mineralogical capacity. Regions under agricultural management and deeper soil layers show the largest undersaturation of mineral-associated carbon. Critically, the degree of undersaturation indicates sequestration efficiency over

years to decades. We show that, across 103 carbon- accrual measurements spanning management interventions globally, soils furthest from their mineralogical capacity are more effective at accruing carbon; sequestration rates average 3-times higher in soils at one tenth of their capacity compared to soils at one half of their capacity. Our findings provide insights into the world's soils, their capacity to store carbon, and priority regions and actions for soil carbon management.

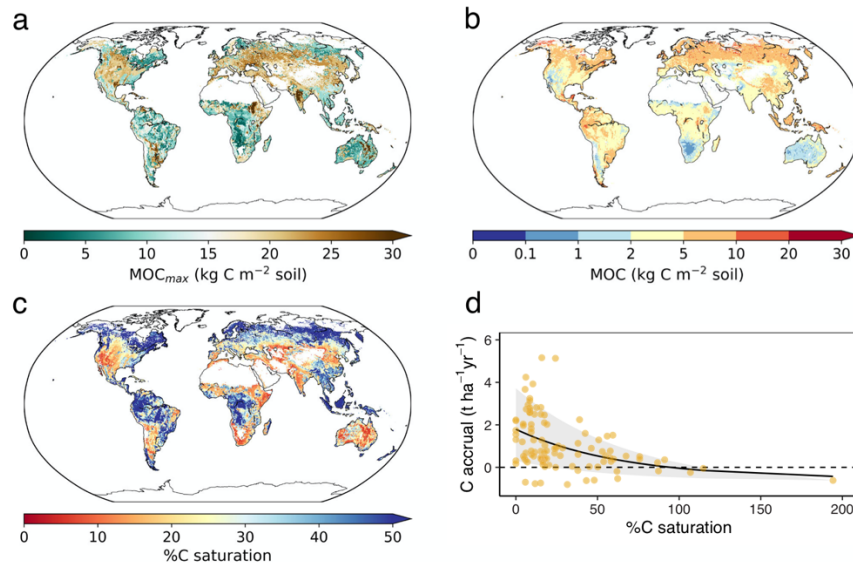


Figure 1. a Mineralogical carbon capacity (MOC_{max} ; $kg\ C\ m^{-2}\ soil$), b mineral-associated organic carbon, and c percent mineralogical carbon saturation (%C saturation) in topsoil (0–30 cm) at 0.5° resolution, excluding tundra, peatlands, and deserts. MOC_{max} was estimated using our data-derived relationships with the amount and type of mineral. MOC was predicted using a random forest model trained on our observational dataset. %C saturation was calculated as MOC/MOC_{max} . Low %C saturation corresponds to a greater C deficit, and therefore highlights regions where targeted soil management could lead to higher C sequestration. d Carbon accrual in topsoil ($t\ ha^{-1}\ yr^{-1}$; mean depth = 29 cm) as a function of %C saturation across sites, based on our global synthesis of studies that measured C accrual following management interventions ($n = 103$). Nonlinear fit depicts asymptotic regression model with shaded areas representing 10th and 90th quantiles.

6. 阿曼钻探项目超镁铁质岩芯的一个新的岩石磁学 分析及其对下地壳和上地幔蚀变的意义

翻译人: 王浩森 11930841@mail.sustech.edu.cn



Hong, G., Till, J.L., Greve, A. et al. New Rock Magnetic Analysis of Ultramafic Cores from the Oman Drilling Project and Its Implications for Alteration of Lower Crust and Upper Mantle [J]. Journal of Geophysical Research: Solid Earth, 2022: e2022JB024379. <https://doi.org/10.1029/2022JB024379>

摘要: 作为阿曼钻井项目的一部分, 为了解大洋岩石圈的磁性, 对从 Wadi Tayin 地块回收的超镁铁质岩石样品进行详细的磁性分析, 为俯冲以来的变化提供了独特的机会。我们检查了横切壳幔边界的 3 个地点 (BA1B、BA3A 和 BA4A) 的 300 至 400 米长的岩芯。橄榄石蚀变中产生少量蛇纹石化的磁铁矿在磁性特征方面起着重要作用。我们的研究揭示了一些新的特征, 这些特征在之前的蛇绿岩研究中还没有报道, 这些研究主要基于表层岩石样品。当蛇纹石化达到某一点 (65%) 时, 磁化率急剧增加。这种模式为在岩石被蛇纹石化时可能发生各种反应(例如, 富铁蛇纹石矿物的进一步水化)引起的磁性矿物的额外产生提供了可能性。一般来说, 最上部 (0 - 40 m) 的敏感性高于较深部分。此外, 纯橄榄岩为主的剖面的磁化率高于方辉橄榄岩组成的剖面。总的来说, 我们的观察表明, 塞梅尔蛇绿岩的地幔岩在不同时期经历了多个蛇纹石化阶段。

ABSTRACT: Detailed magnetic analyses of ultramafic rock samples recovered from the Wadi Tayin massif as part of the Oman Drilling Project provide a unique opportunity to understand the magnetic properties of oceanic lithosphere and its alteration since obduction. We examined 300- to 400-m-long cores from 3 sites (BA1B, BA3A, and BA4A) that transected the crust-mantle boundary. Serpentinization that produces a small amount of magnetite from olivine alteration plays an important role in shaping the magnetic signature of the rocks recovered from these holes. Our investigation reveals new features, which have not been reported in previous studies of ophiolite largely based on surface rock samples. It appears that when serpentinization reaches a certain point

(65%), a sharp increase in magnetic susceptibility occurs. Such pattern opens the possibility of additional production of magnetic minerals induced by various reactions (e.g., further hydration of Fe-rich serpentine minerals), which may have occurred, while the rocks were being serpentinized. In general, the uppermost section (0–40 m) shows higher susceptibility than the deeper part. Also, higher susceptibility is found in dunite-dominated sections than those composed of harzburgite. Overall, our observations suggest that mantle rocks of Semail ophiolite have undergone multiple stages of serpentinization over different time periods.

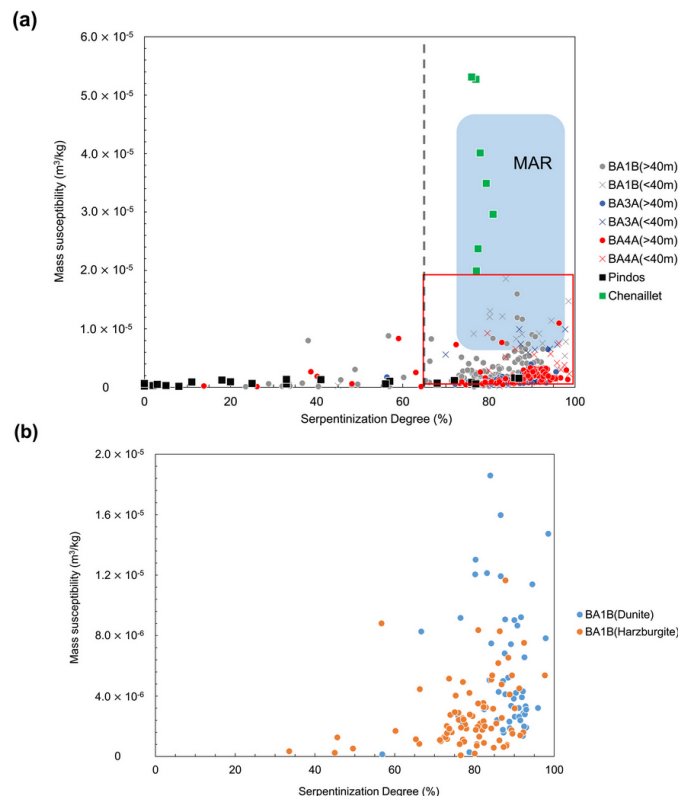


Figure 1. (a) Comparative plot between mass susceptibility and serpentinization degree of Oman Drilling Project holes BA1B, BA3A, and BA4A exhibited with discrete sample data collected from Pindos and Chenaillet ophiolites. Measurements from near-surface (0–40 m depth) samples are shown in crosses. Data from abyssal peridotites of Mid-Atlantic Ridge (MAR) are also noted for reference as a blue cloud. Most of the values measured from OmanDP holes are distributed inside the area encompassed by red lines. The point of 65% serpentinization is highlighted with a dashed line. (b) Plot comparing mass susceptibility versus serpentinization degree of hole BA1B samples of different lithology.

7. 法国南部普罗旺斯二叠纪脊椎动物足迹以及对晚卡匹敦陆地灭绝事件的暗示



翻译人: 张伟杰 12031188@mail.sustech.edu.cn

Marchetti, L., Logghe, A., Mujal, E. et al. *Vertebrate tracks from the Permian of Gonfaron (Provence, Southern France) and their implications for the late Capitanian terrestrial extinction event [J]. Palaeogeography, Palaeoclimatology, Palaeoecology, 2022, 599: 111043.*

<https://doi.org/10.1016/j.palaeo.2022.111043>

摘要: 瓜德鲁普世是四足动物进化的关键时期。它包括兽脚纲动物和立体脊椎动物(后来分别在陆地和淡水环境中占主导地位的类群)最早明确出现以及以及卡匹敦晚期大灭绝事件。这段时期的低纬度动物群,由罕见的四足动物体化石组成,最完整的记录来自法国普罗旺斯盆地的。根据我们修定的分类和地层对比,我们确定 Pelitique 组为晚卡匹敦阶,并将四足鱼类组合归入新定义的组合(Erpetopus 生存带的 Dicynodontipus 亚生存带)。对瓜德鲁普统-乐平统的四足动物群的初步多元统计表明, Pelitique 组鱼群具有典型的 dinocephalian 灭绝后的鱼群组成。它与俄罗斯和南非中纬度至高纬度地区所描述的同时期骨骼动物群相似,可以说是低等纬度地区 dinocephalian 灭绝后恢复的最早证据。我们的研究结果证实了卡匹敦世晚期陆地物种大灭绝的全球性和突发性影响,以及随后在低纬度地区的恢复。这次大灭绝可能与全球性的底栖海洋生物大灭绝在时间上是相等的,而且这两次大灭绝都可能与在 260 Ma 左右达到顶峰的中国峨眉山火山活动引起的气候扰动有关。

ABSTRACT: The Guadalupian was a key epoch for the evolution of tetrapod faunas. It includes the earliest unambiguous occurrences of therapsids and stereospondyls (groups that later became dominant in terrestrial and freshwater environments, respectively) and the late Capitanian mass extinction event. The low-latitude faunas from this time interval, where sufficiently dated, comprise rare tetrapod body fossils whereas the most complete records are provided by ichnoassociations, especially coming from the Provence basins of France. In this paper, we revise the tetrapod ichnoassociation from the Pélitique Formation of the Le Luc Basin of Provence, identifying the following tetrapod ichnotaxa: *Batrachichnus salamandroides* (temnospondyls/lepospondyls),

Capitosauroides talus comb. nov. (therocephalian therapsids), Dicyodontipus isp. (cynodont therapsids), Varanopus isp. (bolosaurian parareptiles), Hyloidichnus bifurcatus (captorhinomorph eureptiles) and Rhynchosauroides isp. (neodiapsid eureptiles). According to our revised ichnotaxonomy and stratigraphic correlations, we date the Pélitique Formation as late Capitanian and assign its tetrapod ichnoassociation to the newly defined Association V (Dicyodontipus sub-biochron of the Erpetopus biochron). The Pélitique Formation ichnoassociation shows a typical composition for a post-dinocephalian extinction ichnofauna, as shown by preliminary multivariate statistics on Guadalupian–Lopingian tetrapod ichnoassociations. It is similar to the contemporaneous skeletal faunas described from the mid- to high-latitude sites of Russia and South Africa and is arguably the earliest evidence of post-dinocephalian extinction recovery at low-latitudes. Our results confirm the global and abrupt impact of the late Capitanian terrestrial mass extinction and the subsequent recovery in the low-latitude realm. This extinction was probably time-equivalent with a global benthic marine mass extinction, and both events may have been linked to climatic perturbation caused by the Emeishian volcanic activity in China, which reached its peak around 260 Ma.

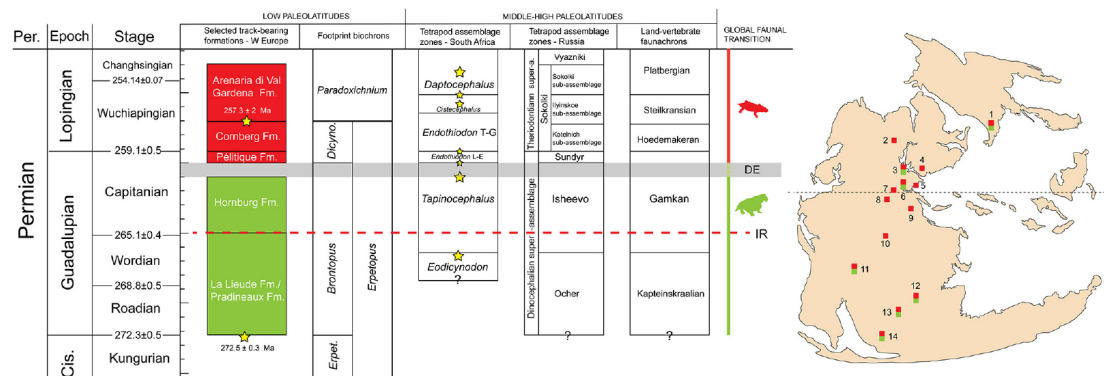


Figure 1. Age and effects of late Capitanian extinction event (Dinocephalian Extinction event – DE) on tetrapod skeleton and footprint record. The event (shaded bar) happened between 259 and 260 Ma and caused a faunal turnover at high (South Africa and Russia) and low (W Europe) palaeolatitudes of Pangaea. The event in W Europe is only recorded by tetrapod footprints, which extend the DE effects globally, at any latitude. 1–14 = significant skeleton and footprint localities. 1 = Russia, 2 = Scotland, 3 = Germany, 4 = Hungary, 5 = Italy, 6 = France, 7 = Spain, 8 = Morocco,

9 = Tunisia, 10 = Niger, 11 = Brazil, 12 = Tanzania, 13 = Zambia, 14 = South Africa. Tetrapod assemblages and land-vertebrate faunachrons follow the studies by Rubidge et al. (2013), Day et al. (2015), Golubev (2015); Sennikov and Golubev (2017), and Lucas (2018); footprint biochrons follow the study by Schneider et al. (2020) but are re-arranged with the new data. Radiometric ages from Zheng et al. (1992), Brauns et al. (2003), Rubidge et al. (2013) and Day et al. (2015). Cis.: Cisuralian. IR = Illawarra reversal. Stars = radiometric dates (see references in the text).

8. 中国西南地区全新世火灾史与气候变化及人类活动有关



翻译人：李海 12031330@mail.sustech.edu.cn

Zijie, Y., Duo, W., Tao, W. et al. *Holocene fire history in southwestern China linked to climate change and human activities [J]. Quaternary Science Reviews, 2022.*

<https://doi.org/10.1016/j.quascirev.2022.107615>

摘要: 近几十年来,全球变暖和人类活动显著增加了人口稠密的亚热带东亚地区的野火风险。然而,在多个时间尺度上导致火灾发生的因素仍不清楚。作者收集并分析了云南高原近 20 年来的火灾观测数据,以及云南高原的滇池、星云湖、齐鲁湖和一龙湖的全新世黑碳记录。作者的目的是探究野火与驱动野火在多个时间尺度上发生的自然和人为变量之间的联系。结果表明:在短时间尺度上,旱季发生森林火灾较多;在长时间尺度上,6~2.8 cal kyr BP 期间湿度降低,森林火灾发生较多;相反,在相对湿润的 11.7~6 cal kyr BP 野火的发生频率相对较低。这些结果表明,在生物燃料丰富的背景下,火灾活动受湿度控制。最低程度的生物质燃烧发生在~2.8 cal kyr BP 之后,这与人为减少生物质可用性有关,尽管干旱程度有所增加。这表明积极的火灾管理和规定的清除措施的重要性,特别是考虑到持续干旱和植被覆盖增加的预测。

ABSTRACT: Global warming and human activities have significantly increased the wildfire risk in highly populated subtropical East Asia over recent decades; however, the factors driving fire occurrence on multiple timescales remain unclear. We present and analyze an observational dataset of fire for the Yunnan Plateau in southwestern China for the past 20 years, together with a Holocene fire history documented by four sedimentary black carbon records from four lakes on the Yunnan Plateau: lakes Dian, Xingyun, Qilu, and Yilong. Our aims were to explore the linkage between wildfires and natural and anthropogenic variables driving wildfire occurrence on multiple timescales. The results show that on a short timescale, more wildfires occurred in drier seasons, and on a longer timescale, more wildfires occurred during 6-2.8 cal kyr BP, when humidity decreased. In contrast, there was a moderate wildfire incidence during the relatively humid interval from 11.7 to 6 cal kyr

BP. These observations indicate that fire activity is controlled by the humidity, against the background of the abundance of biofuel. The lowest degree of biomass burning occurred after ~ 2.8 cal kyr BP and was linked to an anthropogenic reduction of biomass availability, despite an increase in drought. This suggests the importance of active fire management and prescribed clearance measures, especially given projections of continued drought and increased vegetation cover.

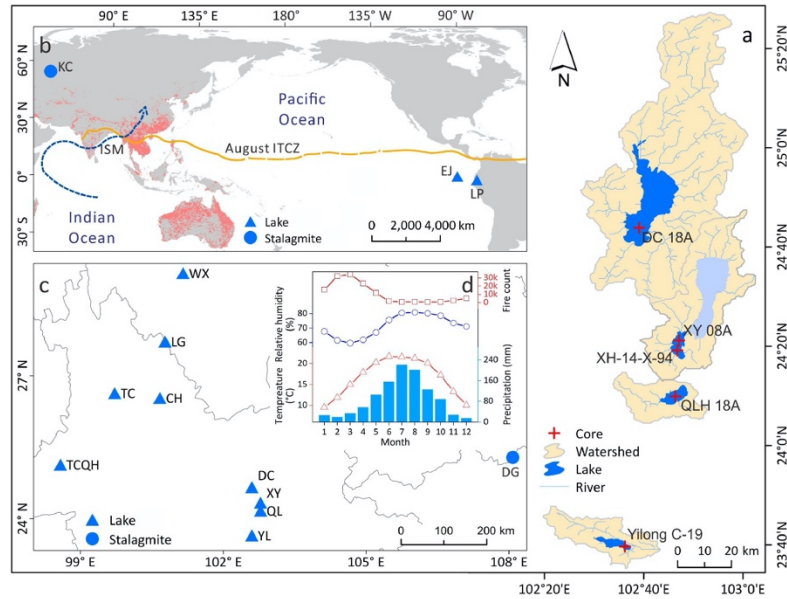


Figure 1. Modern hydrology and climatic status of the study region. (a) Lakes Dian, Xingyun, Qilu and Yilong and their drainage systems. (b) Maps showing the wind direction in the Indian summer monsoon (ISM) domains and the modern location of the Intertropical Convergence Zone in August (ITCZ). Also shown is the location of the study area against the background of global fire ignition for 2003-2016. (c) Locations of records in the surrounding region mentioned in the text. (d) Monthly summed fire count, relative humidity, precipitation and temperature during 2001-2020.

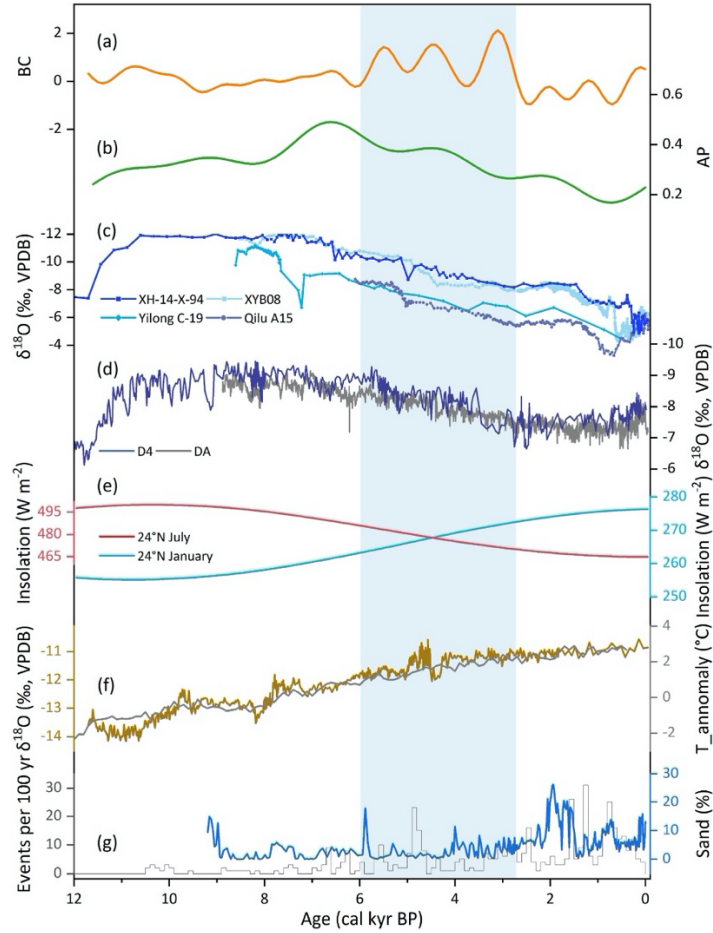


Figure 2. Compilation Holocene fire history in southwestern China and its possible forcing mechanism. (a) Integrated BC record smoothed with a 0.00125 Hz low pass FFT filter. (b) Record of the proportion of arboreal pollen (AP) smoothed with a 0.5 Hz low pass FFT filter. (c) Carbonate $\delta^{18}\text{O}$ records from lakes Xingyun, Qilu, and Yilong. (d) Speleothem $\delta^{18}\text{O}$ record from Dongge Cave. (e) July (red line) and December (blue line) insolation at 24°N . (f) Winter temperature simulation of the CCSM3 model and reconstruction from Kinderlinskaya Cave. (g) Number of ENSO events per 100 years (grey line) and a record of the sedimentary sand content from Lake El Junco in South America (blue line). (For interpretation of the references to colour in this figure legend, the reader is referred to the Web version of this article.)

9. 末次冰期太平洋水体在塔斯曼深部的外流

翻译人：张亚南 zhangyn3@mail.sustech.edu.cn



Struve, T., Wilson, D.J., Hines, S.K.V. et al. A deep Tasman outflow of Pacific waters during the last glacial period [J]. Nature Communications, 2022, 13, 3763.

<https://doi.org/10.1038/s41467-022-31116-7>

摘要：海洋间的水团交换是通过德雷克海峡、印度尼西亚海域、非洲南部和塔斯马尼亚南部的关键海洋咽喉点的流量来调节的。文中，作者利用中深度（1460–1689m）冷水珊瑚骨架的钕同位素（ ϵ_{Nd} ）来追踪塔斯马尼亚南部环流在末次冰期的变化。 ϵ_{Nd} 数据在末次冰期和 HS 1 时期趋于 ~ -4.6 ，与同时期的南大洋 ϵ_{Nd} 值（ ~ -7 ）明显不同。结合先前发表的放射性碳数据，文中的结果表明在这些时期存在着一个具有独特 ϵ_{Nd} 值得年轻水团。这种情况可以用更强烈得太平洋翻转环流来解释，支持了太平洋深水（包括北太平洋中层水）在塔斯曼海的溢流。

ABSTRACT: The interoceanic exchange of water masses is modulated by flow through key oceanic choke points in the Drake Passage, the Indonesian Seas, south of Africa, and south of Tasmania. Here, we use the neodymium isotope signature (ϵ_{Nd}) of cold-water coral skeletons from intermediate depths (1460–1689 m) to trace circulation changes south of Tasmania during the last glacial period. The key feature of our dataset is a long-term trend towards radiogenic ϵ_{Nd} values of ~ -4.6 during the Last Glacial Maximum and Heinrich Stadial 1, which are clearly distinct from contemporaneous Southern Ocean ϵ_{Nd} of ~ -7 . When combined with previously published radiocarbon data from the same corals, our results indicate that a unique radiogenic and young water mass was present during this time. This scenario can be explained by a more vigorous Pacific overturning circulation that supported a deeper outflow of Pacific waters, including North Pacific Intermediate Water, through the Tasman Sea.

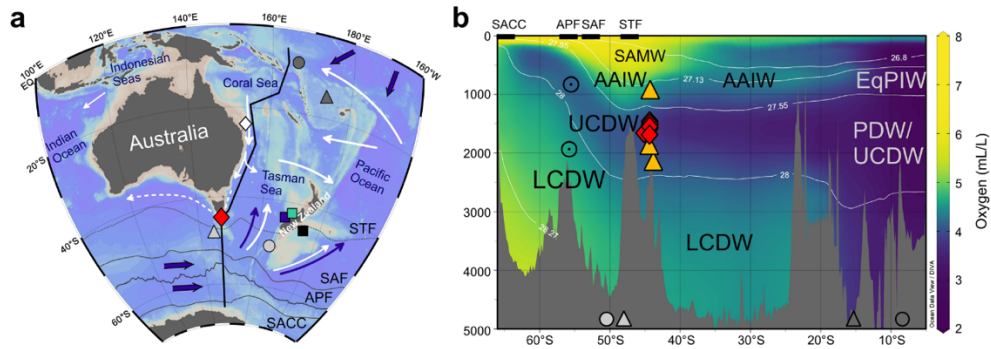


Figure 1. Coral sample locations and regional hydrography. a Map showing the coral sample locations south of Tasmania (red diamond) and locations of seawater Nd isotope profiles from stations SR3-60 (light gray triangle), TAN0803-41 (light gray circle), GeoB17019-1 (dark gray triangle), and GeoB17018-1 (dark gray circle). Solid white arrows indicate simplified flow paths of intermediate waters, while the dashed arrow indicates the Tasman Leakage, and dark blue arrows represent deep water flow. The mean positions of the Subtropical Front (STF), Subantarctic Front (SAF), Antarctic Polar Front (APF), and Southern ACC front (SACC) are indicated by gray lines. Colored squares indicate locations of important paleoceanographic records from sediment cores MD06-2986 (dark blue, 1477 m water depth), SO136-003GC (green, 944 m water depth), and MD97-2120 (black, 1210 m water depth). The white diamond indicates the location of core FR1/97 GC-12 (990 m water depth). b Oxygen concentration section (along the black line in a), highlighting the major subsurface water masses in the study area: Subantarctic Mode Water (SAMW), Antarctic Intermediate Water (AAIW), Upper Circumpolar Deep Water (UCDW), Lower Circumpolar Deep Water (LCDW), Pacific Deep Water (PDW), and Equatorial Pacific Intermediate Water (EqPIW) representing a mixture of AAIW originating from the Southeast Pacific and upwelled PDW. Thin black lines indicate surfaces of neutral density anomalies γ_n (in kg/m^3). Yellow triangles and red diamonds depict sampling depths of modern and fossil corals, respectively. Ocean fronts and locations of water column profiles (gray circles and triangles) as in a. Base map in a and oxygen section in b generated with ODV software.

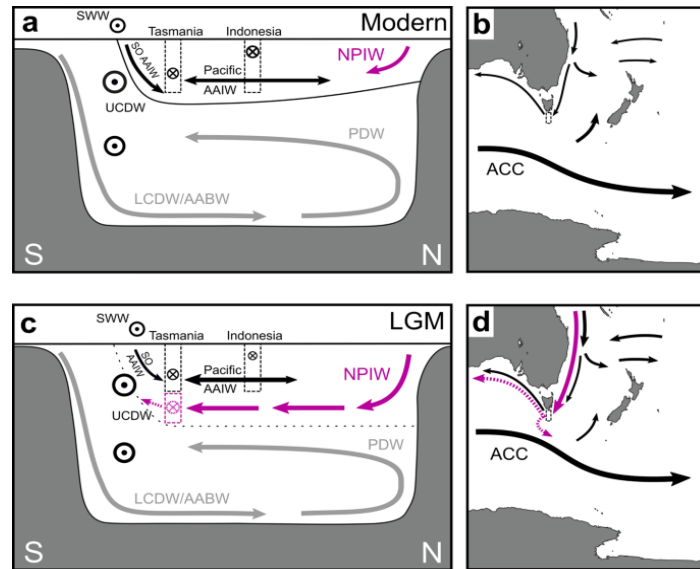


Figure 1. Schematic of inferred circulation changes between the modern-day and the Last Glacial Maximum (LGM). Cross-sections show the Pacific Ocean circulation for a the modern-day and c the LGM. Maps focus on the intermediate-depth circulation in the study area near Tasmania for b the present-day (see also Fig. 1a) and d the LGM. Base maps in b, d produced with ODV software. Water mass pathways are indicated by arrows: Antarctic Intermediate Water (AAIW, black) and North Pacific Intermediate Water (NPIW, purple). SO: Southern Ocean. Note that the eastward flow of the Antarctic Circumpolar Current (ACC) (circled dots in a and c) comprises also Upper Circumpolar Deep Water (UCDW) and Lower Circumpolar Deep Water (LCDW) (see also Fig. 1b for more details). Note also that the two possible pathways of glacial Tasman outflow waters are indicated by stippled lines in c, d and that the purple arrows in c, d do not represent pure NPIW, since it is influenced by the admixture of other ambient water masses during its southwards transport (see main text). Gray arrows in a, c indicate the deep overturning, where upwelling of LCDW and Antarctic Bottom Water (AABW) feeds into the southward return flow of Pacific Deep Water (PDW). Flow strengths are schematically represented by the thickness of arrows (meridional flows) or the size of the circled dots/crosses (zonal flows). The solid black line in a represents the intermediate water layer ventilated primarily by AAIW and NPIW in the modern Pacific Ocean, while the stippled black line in c indicates the deepened LGM analogue. Dashed boxes indicate the locations and approximate depth extents of Pacific outflow along the Tasman margin and through the Indonesian Seas. The position of the Southern Westerly Winds (SWW) is also shown with circled dots.

10. 晚全新世中国北方半干旱地区植被变化从自然向人为强迫的过渡

翻译人：刘宇星 11811211@mail.sustech.edu.cn



Ding, G., Chen, J., Yan, H. et al. *Late Holocene transition from natural to anthropogenic forcing of vegetation change in the semi-arid region of northern China [J]. Quaternary Science Reviews*, 2022, 287: 107561.

<https://doi.org/10.1016/j.quascirev.2022.107561>

摘要：了解全新世植被对气候变化和人类活动的响应可能有助于预测植被变化的未来轨迹。此外，在中国北方半干旱地区，也可能为解决生态问题和实现可持续发展目标提供科学依据。基于 5 个 AMS ^{14}C 年代和 259 份来自中国陕西省沟池湖沉积物的化石花粉样本，我们重建了中全新世以来季风边缘地区植被演替的格局和过程。结合区域季风降水记录和考古数据，我们利用结果评估植被、气候变化和人类活动之间关系的变化。8-1 ka (1 ka = 1000 cal a BP, BP = before present, 其中“现在”是公元 1950 年) 的植被发育主要受自然气候变化的控制。最佳植被条件出现在 7.8~5.3 ka 期间，此时季风降水最强。这段时期的植被主要是有蒿草的草地。同时，湿生植物的百分比达到最大值。5.3~1 k 期间，季风降水减少，旱生植物比例增加，湿生植物比例下降。在~1 ka 之后，人类活动成为植被变化的主要驱动力。旱生植物的比例在中世纪暖期 (MWP, 公元 1000-1300 年) 有所增加，而湿生植物的比例在小冰期早期 (LIA, 公元 1400-1900 年) 有所增加。这表明 MWP 的潮湿气候和 LIA 的干旱气候之间的转变对植被的影响相对较小。大约 1 ka 后，人类引起的花粉显著增加，同时在 Gouchi 湖的沉积物积累速率增加。因此，人类活动很可能早在 1000 年前就开始显著影响区域植被的演化。综合中国植被变化从自然强迫到人为强迫转变的时间，揭示了明显的空间差异。在中国北方，从~2-1 ka (尤其是从 1 ka 开始) 人类活动开始主导植被变化，而在中国南方，人类对植被的显著影响发生得更早 (~5-3 ka)。未来，在中国北方气候干燥和人类活动进一步加剧的综合作用下，实施科学的环境规划，恢复区域植被，促进该地区的生态系统的可持续发展将变得越来越重要。

ABSTRACT: Understanding the vegetation response to climate change and human activities during the Holocene may help predict the future trajectory of vegetation change. Moreover, in the semi-

arid region of northern China, it may also provide a scientific basis for addressing ecological problems and achieving sustainable development goals. Based on 5 AMS ^{14}C dates and 259 fossil pollen samples from the sediments of Lake Gouchi in Shaanxi Province, China, we reconstructed the pattern and process of vegetation succession in the monsoon margin area since the mid-Holocene. Combined with records of regional monsoonal precipitation and archaeological data, we use the results to evaluate changes in the relationship between vegetation, climate change and human activities. The vegetation development during 8–1 ka (1 ka = 1000 cal a BP, BP = before present, where “present” is 1950 AD) was mainly controlled by natural climate change. Optimum vegetation conditions occurred during 7.8–5.3 ka when the monsoon precipitation was the strongest. The vegetation during this interval was mainly grassland with *Artemisia*. Meanwhile, the percentage of hygrophytes reached its maximum. During 5.3–1 ka, the monsoon precipitation decreased and the proportion of xerophytes increased, while the proportion of hygrophytes decreased. After ~1 ka, human activities became the dominant driver of vegetation change. The proportion of xerophytes increased during the Medieval Warm Period (MWP, 1000–1300 AD), while the proportion of hygrophytes increased during the early stage of the Little Ice Age (LIA, 1400–1900 AD). This suggests that the shifts between the humid climate of the MWP and the arid climate of the LIA had relatively little influence on the vegetation. The pollen of anthropochores increased substantially after ~1 ka, together with an increase in the sediment accumulation rate at Lake Gouchi. Thus, it is likely that human activity began to significantly affect the evolution of the regional vegetation as early as ~1000 years ago. A synthesis of the timing of the transition from natural to anthropogenic forcing of vegetation change in China reveals pronounced spatial differences. In northern China human activity began to dominate vegetation change from ~2 to 1 ka (especially since 1 ka), while in southern China, a significant human impact on the vegetation occurred much earlier, during ~5–3 ka. In the future, under the combined effects of a drying climate and the further intensification of human activities in northern China, it will become increasingly important to implement science-based environmental planning in order to restore the regional vegetation and promote the sustainable development of the terrestrial ecosystems of the region.

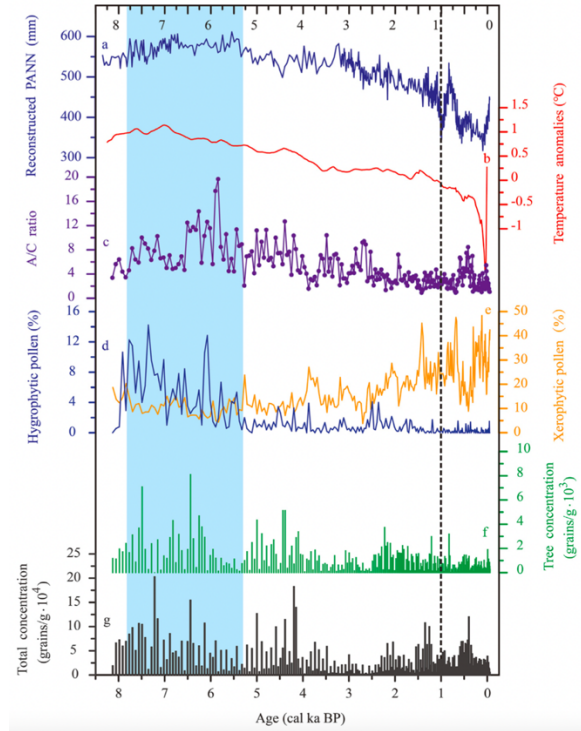


Figure 1. Selected paleoenvironmental indicators from core GC15B from Lake Gouchi and comparison with regional paleoenvironmental records. (a). Pollen-based quantitative annual precipitation records from Lake Gonghai. (b) Synthesized Northern Hemisphere temperature. (c) Ratio of Artemisia to Chenopodiaceae (A/C) pollen at Lake Gouchi. (d). Total hygrophyte pollen at Lake Gouchi. (e). Total xerophyte pollen at Lake Gouchi. (f) Tree pollen concentration at Lake Gouchi. (g). Total pollen concentration at Lake Gouchi.

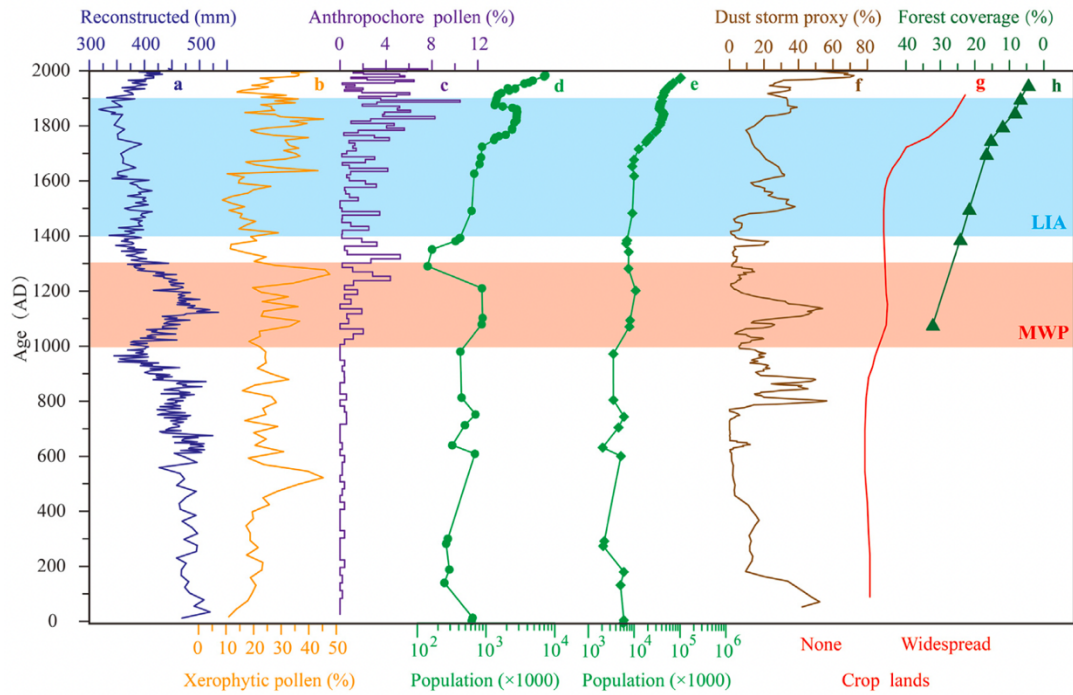


Figure 2. Comparison of pollen indicators of disturbance and cultivation from Lake Gouchi with records of regional climate change and human activity. (a) Pollen-based quantitative precipitation reconstruction from Lake Gonghai. (b) Total xerophyte pollen from Lake Gouchi. (c) Pollen record of anthropochores from Lake Gouchi. (d) Human population of the study area (Shaanxi, Ningxia, Gansu and Inner Mongolia). (e) Human population of China. (f) Dust storm record from Lake Gonghai. (g) Changes in the cultivated area of the Chinese Loess Plateau. (h) Changes in the forest cover of the Chinese Loess Plateau.